Internal non-equilibrium studied by RF pulses in the system of three nuclear $^{1}/_{2}$ spins

1989 J. Phys.: Condens. Matter 1 9219

(http://iopscience.iop.org/0953-8984/1/46/014)

J. Phys.: Condens. Matter 1 (1989) 9219–9229. Printed in the UK

Internal non-equilibrium studied by RF pulses in the system of three nuclear $\frac{1}{2}$-spins

A H Vuorimäki and M Punkkinen
Wihuri Physical Laboratory and Department of Physical Sciences, University of Turku, SF-20500 Turku, Finland

Received 21 March 1989, in final form 22 May 1989

Abstract. Free-induction decays following a single RF pulse as well as the pulse sequence θ_x–t_1–θ_{-x}–t_2–θ' are studied for a symmetric system of three identical spin-$\frac{1}{2}$ nuclei. When the three-pulse sequence is applied to the sample at thermal equilibrium, the spin system after the first two pulses usually does not obey a spin temperature but can be described by energy-level populations. Analytical expressions relating the Fourier spectra of the decays to the populations and the pulse lengths are derived. Calculations are compared to experimental methyl-proton lineshapes in a $CH_3COONa \cdot 3D_2O$ single crystal.

1. Introduction

Nuclear spin systems are usually investigated at internal equilibrium, i.e. in a state that can be described by a spin temperature. The shape of the free-induction decay (FID) following an RF pulse is then independent of the angle by which the pulse has rotated the magnetisation. In this case the Fourier transform of the decay is identical to the absorption curve obtained by the slow passage of a continuous RF field [1]. The spin temperature can be made non-uniform by chemical reactions, continuous RF fields or strong RF pulses. If the populations of the energy levels of a system with the total nuclear spin $I > \frac{1}{2}$ cannot be described by a Boltzmann distribution, the relation between the FID and the absorption no longer holds [2]. Nor can many-pulse experiments on a multi-level system be described by precessing magnetisation vectors. To handle such cases, more sophisticated, general treatments are developed [3]. For systems whose eigen-functions are known, however, a straightforward quantum mechanical approach is also applicable and relates the observable FID shape to the level populations by analytical expressions.

We have studied the system of three dipolar coupled spin-$\frac{1}{2}$ nuclei forming a one-dimensional rotor like the protons belonging to methyl groups in molecular crystals. The results of calculations concerning the pulse sequence θ_x–t_1–θ_{-x}–t_2–θ' were compared to experiments on a CF_3COOAg single crystal in a recent Letter [4]. In this paper we give the theory in more detail and present new experimental results on a more favourable test compound, $CH_3COONa \cdot 3D_2O$.

2. Theory

The system of interest consists of three spin-$\frac{1}{2}$ nuclei arranged in the form of an equilateral

0953-8984/89/469219 + 11 $02.50

triangle. The triangle undergoes hindered rotation or reorientation about its threefold axis which makes an angle ϕ with the external magnetic field $\boldsymbol{B}_0$.

The rotor-spin eigenfunctions Ψ_{Xm} of this system can be labelled by $X_m = A_{\pm 3/2}$, $A_{\pm 1/2}$, $E^a_{\pm 1/2}$ and $E^b_{\pm 1/2}$ according to the irreducible representations of the cyclic point group C_3 and the z component of the total nuclear spin [5, 6]. At low temperatures the tunneling splitting $\hbar\omega_t$ of the rotational ground state becomes important if the nuclei are light and the hindering potential is weak. Then the E levels are raised by $\frac{1}{3}\hbar\omega_t$ and the A levels lowered by $\frac{2}{3}\hbar\omega_t$ [5, 7]. This splitting is not usually seen directly in the NMR spectrum, because the RF field cannot induce transitions between different symmetry species.

For lineshapes it is more important that the energy levels are shifted by the dipole–dipole interaction between the three nuclei [8]. Unless $\phi = 0°$ the A and E levels are mixed. If, however, the reorientation is fast or the tunneling frequency ω_t is large, there is practically no mixing and the eight eigenstates X_m are acceptable to first order [6, 9]. In these cases E levels are unperturbed, but $A_{\pm 3/2}$ levels are shifted upwards and $A_{\pm 1/2}$ levels downwards by $d = (\mu_0/4\pi)(3\gamma^2\hbar^2/8r^3)(3\cos^2\phi - 1)$, where r is the side length of the triangle and γ the magnetogyric ratio of the nuclei. The equilibrium spectrum of the system then consists of the central line at $\omega_0 = \gamma B_0$ and satellites separated from it by $\pm 2d/\hbar$. If all the nuclear triangles have equal ϕ, the intensities of the three lines are in the ratio 1:2:1. This can be readily calculated from the matrix elements of the operator I_+ (cf. the expressions (3) below).

2.1. Free-induction decay

We derive the main features of FID following a single RF pulse assuming that the system has initial populations N_{Xm} corresponding to its eight levels X_m. Our treatment is basically similar to those performed for a spin-$\frac{3}{2}$ nucleus with a quadrupolar splitting [10, 11].

The calculations are carried out in the frame rotating at the angular frequency ω of the RF field of the spectrometer. During a pulse of amplitude ω_1/γ along the x axis, the spin Hamiltonian of the system is [12]

$$\mathcal{H} = \hbar(\omega - \omega_0)I_z + \mathcal{H}_d - \hbar\omega_1 I_x. \tag{1}$$

Here I_z and I_x are components of the operator of the total nuclear spin for the three nuclei and $\mathcal{H}_d$ is the secular part of the time-averaged dipolar interaction between the spins. The wavefunction, expressed as a combination of the eigenfunctions ψ_{Xm}, is

$$\Psi(t) = \sum_{X,m} C_{Xm}(t)\exp(-i\omega_{Xm}t)\,\Psi_{Xm} \tag{2}$$

where $\hbar\omega_{Xm} = \hbar(\omega - \omega_0)m + d\delta_{XA}(\delta_{|m|3/2} - \delta_{|m|1/2})$ are the spin energies in the rotating frame. The weights $C_{Xm}(t)$ are constant before and after the pulse, because we ignore the attenuation by longitudinal and transverse relaxation. We also omit the offset by tuning $\omega = \omega_0$.

By substituting (1) and (2) into the time-dependent Schrödinger equation $i\hbar(d/dt)\Psi(t) = \mathcal{H}\Psi(t)$ and using the relations

$$\begin{aligned}
&\langle\psi_{A\pm 3/2}|I_\pm|\psi_{A\pm 1/2}\rangle = \sqrt{3}\\
&\langle\psi_{A\pm 1/2}|I_\pm|\psi_{A\mp 1/2}\rangle = 2\\
&\langle\psi_{E^x\pm 1/2}|I_\pm|\psi_{E^x\mp 1/2}\rangle = -1\\
&\langle\psi_{X'm'}|I_\pm|\psi_{Xm}\rangle = 0 \qquad X' \neq X \text{ or } m' \neq m \pm 1
\end{aligned} \tag{3}$$

where x denotes a or b, we get

$$\begin{aligned}(\mathrm{d}/\mathrm{d}t)C_{\mathrm{A}\pm 3/2} &= \mathrm{i}\omega_1(\tfrac{1}{2}\sqrt{3})C_{\mathrm{A}\pm 1/2}\exp(\mathrm{i}2dt/\hbar)\\ (\mathrm{d}/\mathrm{d}t)C_{\mathrm{A}\pm 1/2} &= \mathrm{i}\omega_1[(\tfrac{1}{2}\sqrt{3})C_{\mathrm{A}\pm 3/2}\exp(-\mathrm{i}2dt/\hbar) + C_{\mathrm{A}\mp 1/2}]\\ (\mathrm{d}/\mathrm{d}t)C_{\mathrm{E}^{\mathrm{x}}\pm 1/2} &= -\mathrm{i}\omega_1\tfrac{1}{2}C_{\mathrm{E}^{\mathrm{x}}\mp 1/2}\,.\end{aligned} \tag{4}$$

During a sufficiently strong RF pulse with $\hbar\omega_1 \gg d$ the solution of (4) will be

$$\begin{aligned}C_{\mathrm{A}\pm 3/2}(t) &= \pm A_1\sqrt{3}\exp(\mathrm{i}\tfrac{1}{2}\omega_1 t) - A_2\sqrt{3}\exp(-\mathrm{i}\tfrac{1}{2}\omega_1 t) + A_3\sqrt{\tfrac{1}{3}}\exp(\mathrm{i}\tfrac{3}{2}\omega_1 t)\\ &\quad \mp A_4\sqrt{\tfrac{1}{3}}\exp(-\mathrm{i}\tfrac{3}{2}\omega_1 t)\\ C_{\mathrm{A}\pm 1/2}(t) &= \pm A_1\exp(\mathrm{i}\tfrac{1}{2}\omega_1 t) + A_2\exp(-\mathrm{i}\tfrac{1}{2}\omega_1 t) + A_3\exp(\mathrm{i}\tfrac{3}{2}\omega_1 t)\\ &\quad \pm A_4\exp(-\mathrm{i}\tfrac{3}{2}\omega_1 t)\\ C_{\mathrm{E}^{\mathrm{x}}\pm 1/2}(t) &= \pm B_1^{\mathrm{x}}\exp(\mathrm{i}\tfrac{1}{2}\omega_1 t) + B_2^{\mathrm{x}}\exp(-\mathrm{i}\tfrac{1}{2}\omega_1 t)\end{aligned} \tag{5}$$

with coefficients

$$\begin{aligned}A_{1,2} &= \tfrac{1}{8}[-\sqrt{3}C_{\mathrm{A}-3/2}(0) \pm C_{\mathrm{A}-1/2}(0) + C_{\mathrm{A}1/2}(0) \pm \sqrt{3}C_{\mathrm{A}3/2}(0)]\\ A_{3,4} &= \tfrac{1}{8}[\sqrt{3}C_{\mathrm{A}-3/2}(0) \pm 3C_{\mathrm{A}-1/2}(0) + 3C_{\mathrm{A}1/2}(0) \pm \sqrt{3}C_{\mathrm{A}3/2}(0)]\\ B_{1,2}^{\mathrm{X}} &= \tfrac{1}{2}[\mp\sqrt{3}C_{\mathrm{E}^{\mathrm{x}}-1/2}(0) + C_{\mathrm{E}^{\mathrm{x}}1/2}(0)].\end{aligned} \tag{6}$$

Here the first subscript corresponds to the upper sign and the second to the lower sign. $C_{\mathrm{X}m}(0)$ is the value of $C_{\mathrm{X}m}(t)$ just before the pulse. The condition $\hbar\omega_1 \gg d$ was well fulfilled in our experiments. However, for $\hbar\omega_1$ not very much larger than d a more accurate result is presented in [13].

At the end of the pulse with length t_{p} the weights in the wavefunction (2) are $C_{\mathrm{X}m}(t_{\mathrm{p}})$. In the laboratory frame the wavefunction is transformed to $\exp(\mathrm{i}\omega_0 t I_z)\Psi(t)$ and the FID observed is proportional to the expectation value of I_y which is the imaginary part of

$$\begin{aligned}&\sqrt{3}\langle C_{\mathrm{A}3/2}(t_{\mathrm{p}})^*\, C_{\mathrm{A}1/2}(t_{\mathrm{p}})\rangle\exp[-\mathrm{i}(\omega_0 - 2d/\hbar)t]\\ &\quad + 2\langle C_{\mathrm{A}1/2}(t_{\mathrm{p}})^*\, C_{\mathrm{A}-1/2}(t_{\mathrm{p}})\rangle\exp[-\mathrm{i}\omega_0 t]\\ &\quad + \sqrt{3}\langle C_{\mathrm{A}-1/2}(t_{\mathrm{p}})^*\, C_{\mathrm{A}-3/2}(t_{\mathrm{p}})\rangle\exp[-\mathrm{i}(\omega_0 + 2d/\hbar)t]\\ &\quad - \langle C_{\mathrm{E}^{\mathrm{a}}1/2}(t_{\mathrm{p}})^*\, C_{\mathrm{E}^{\mathrm{a}}-1/2}(t_{\mathrm{p}})\rangle\exp[-\mathrm{i}\omega_0 t]\\ &\quad - \langle C_{\mathrm{E}^{\mathrm{b}}1/2}(t_{\mathrm{p}})^*\, C_{\mathrm{E}^{\mathrm{b}}-1/2}(t_{\mathrm{p}})\rangle\exp[-\mathrm{i}\omega_0 t].\end{aligned} \tag{7}$$

By the hypothesis of random phases the ensemble averages of the various terms in (7) will be $\langle C_{\mathrm{X}m}(0)^*\, C_{\mathrm{X}'m'}(0)\rangle = \delta_{\mathrm{XX}'}\delta_{mm'}N_{\mathrm{X}m}/N$, where $N = \Sigma_{\mathrm{X}m}N_{\mathrm{X}m}$. The substitution of (5) and (6) into (7) gives for FID

$$\langle I_y\rangle = M_-\cos(\omega_0 - 2d/\hbar)t + M_{\mathrm{c}}\cos\omega_0 t + M_+\cos(\omega_0 + 2d/\hbar)t \tag{8}$$

where the amplitudes are given by the products

$$M_\pm = \boldsymbol{p}\mathbf{M}_\pm\boldsymbol{n}^{\mathrm{T}} \qquad M_{\mathrm{c}} = \boldsymbol{p}\mathbf{M}_{\mathrm{c}}\boldsymbol{n}^{\mathrm{T}}. \tag{9}$$

Here $\boldsymbol{p}$ is the vector

$$\boldsymbol{p} = (\sin\theta, \sin 2\theta, \sin 3\theta), \tag{10}$$

$\boldsymbol{n}^{\mathrm{T}}$ the transpose of the vector

$$\boldsymbol{n} = (n_{\mathrm{A}-3/2}, n_{\mathrm{A}-1/2}, n_{\mathrm{A}1/2}, n_{\mathrm{A}3/2}, n_{\mathrm{E}^{\mathrm{a}}-1/2}, n_{\mathrm{E}^{\mathrm{a}}1/2}, n_{\mathrm{E}^{\mathrm{b}}-1/2}, n_{\mathrm{E}^{\mathrm{b}}1/2}) \tag{11}$$

and $\mathbf{M}_\pm$ and $\mathbf{M}_c$ are matrices

$$\mathbf{M}_\pm = \tfrac{1}{32}\begin{bmatrix} -15 & -3 & 3 & 15 & 0 & 0 & 0 & 0 \\ \mp 12 & \pm 12 & \pm 12 & \mp 12 & 0 & 0 & 0 & 0 \\ -3 & 9 & -9 & 3 & 0 & 0 & 0 & 0 \end{bmatrix}$$

$$\mathbf{M}_c = \tfrac{1}{32}\begin{bmatrix} -18 & -10 & 10 & 18 & -16 & 16 & -16 & 16 \\ 0 & 0 & 0 & 0 & 0 & 0 & 0 & 0 \\ 6 & -18 & 18 & -6 & 0 & 0 & 0 & 0 \end{bmatrix}. \tag{12}$$

The vector $\boldsymbol{p}$ depends only on the angle $\theta = \omega_1 t_p$ which in the classical picture describes the rotation of the magnetisation by the pulse. The excess populations n_{Xm} in the vector $\boldsymbol{n}$ are related to the instantaneous populations N_{Xm} by $n_{Xm} \equiv N_{Xm}N - \frac{1}{8}$. (Note, however, that $N_A \equiv \Sigma_m N_{Am}$ and $N_E \equiv N_{E^a} + N_{E^b} \equiv \Sigma_m N_{E^a m} + \Sigma_m N_{E^b m}$ are not equal if $\omega_t \neq 0$.) The Fourier transform of the FID envelope (8) is a spectrum composed of a central line at ω_0 with amplitude M_c and satellites at $\omega_0 \pm 2d/\hbar$ with amplitudes $M_\pm$.

If all the levels have a common spin temperature or at least if each symmetry species X has its own spin temperature T_X, then the shape of the spectrum (9) does not depend on the angle θ. Substituting $n_{Xm} = m\hbar\omega_0/8kT_X$ into (11) gives

$$\begin{aligned} M_+ &= M_- = (3/T_A)(\hbar\omega_0/16k)\sin\theta \\ M_c &= (4/T_A + 1/T_{E^a} + 1/T_{E^b})(\hbar\omega_0/16k)\sin\theta. \end{aligned} \tag{13}$$

This holds precisely for $\omega_t = 0$. For a non-vanishing tunneling splitting the correct excess populations are $n_{Xm} = (m\hbar\omega_0/8kT_X)(2N_X/N) + \frac{1}{8}(2N_X/N - 1)$, where $N_A/N_E = \exp(\hbar\omega_t/kT_{latt})$. If $\hbar\omega_t/k$ is comparable to the lattice temperature T_{latt}, (13) should be replaced by a more complicated expression.

If no spin temperature can be attributed to the A levels, the shape of the spectrum depends on the pulse angle. Only when θ is small does the Fourier spectrum (9) agree with the real, unsaturated absorption curve. After a 90° pulse, on the other hand, $M_+ = M_-$ independently of the initial populations, hence preventing the observation of any dipolar energy.

2.2. *Pulse sequence* θ_x–t_1–θ_{-x}–t_2–θ'

To create internal non-equilibrium states in the three-spin system without producing any dipolar energy we apply two RF pulses of equal length but opposite phases. Our pulse pair θ_x–t_1–θ_{-x} is a generalisation of the pair $90°_x$–t_1–$90°_{-x}$ used to decrease the weight of the faster decaying component in systems containing two kinds of spins with different decay rates for transverse magnetisation [14, 15]. It was because the components in the earlier experiments originated from nuclei belonging to different sublattices [14] or different symmetry species [15] that the corresponding magnetisations could be described by separate vectors. In our case the components are attributed to different resonances of the same spin isomer ($I = \frac{3}{2}$) making the vector model unapplicable.

We calculate the effect of the pulse pair θ_x–t_1–θ_{-x} on the level populations N_{Xm} of the three-spin system. After the first pulse the state of the system is described by (2) with weights $C_{Xm}(t_p)$ from (5). If all attenuation during the interval t_1 is ignored, the initial values of the weights at the beginning of the second pulse are $C_{Xm}(t_p)\exp(-i\omega_{Xm}t_1)$.

The evolution during θ_{-x} is similar to that during the first pulse except for the replacement of ω_1 by $-\omega_1$ in the Hamiltonian (1). By using (5) and (6) we obtain for the weights at the end of the θ_{-x} pulse

$$\begin{aligned}
C'_{A\pm3/2} &= [1 - \tfrac{3}{2}\sinh(i dt_1/\hbar)\sinh^2(i\omega_1 t_p)]C_{A\pm3/2}(0) \\
&\quad - \tfrac{1}{2}\sqrt{3}\sinh(i dt_1/\hbar)\sinh^2(i\omega_1 t_p)C_{A\mp1/2}(0) \\
&\quad -\tfrac{1}{2}\sqrt{3}\sinh(i dt_1/\hbar)\sinh(i2\omega_1 t_p)C_{A\pm1/2}(0) \\
C'_{A\pm1/2} &= [\exp(i dt_1/\hbar) + \tfrac{3}{2}\sinh(i dt_1/\hbar)\sinh^2(i\omega_1 t_p)]C_{A\pm1/2}(0) \\
&\quad - \tfrac{1}{2}\sqrt{3}\sinh(i dt_1/\hbar)\sinh^2(i\omega_1 t_p)C_{A\mp3/2}(0) \\
&\quad +\tfrac{1}{2}\sqrt{3}\sinh(i dt_1/\hbar)\sinh(i2\omega_1 t_p)C_{A\pm3/2}(0) \\
C'_{E^x\pm3/2} &= C_{E^x\pm1/2}(0).
\end{aligned} \tag{14}$$

Randomness in the phases of $C_{Xm}(0)$ is used to calculate the new level populations $N'_{Xm} = \langle |C'_{Xm}|^2 \rangle$. The new excess populations n'_{Xm} are given by the vector formula

$$n'^{T} = \mathbf{M}_\theta n^T \tag{15}$$

where

$$\mathbf{M}_\theta = \begin{bmatrix}
1-a-b & a & b & 0 & 0 & 0 & 0 & 0 \\
a & 1-a-b & 0 & b & 0 & 0 & 0 & 0 \\
b & 0 & 1-a-b & a & 0 & 0 & 0 & 0 \\
0 & b & a & 1-a-b & 0 & 0 & 0 & 0 \\
0 & 0 & 0 & 0 & 1 & 0 & 0 & 0 \\
0 & 0 & 0 & 0 & 0 & 1 & 0 & 0 \\
0 & 0 & 0 & 0 & 0 & 0 & 1 & 0 \\
0 & 0 & 0 & 0 & 0 & 0 & 0 & 0
\end{bmatrix} \tag{16}$$

$$\begin{aligned}
a &= 3\sin^2(dt_1/\hbar)\sin^2\theta\cos^2\theta \\
b &= \tfrac{3}{4}\sin^2(dt_1/\hbar)\sin^4\theta.
\end{aligned} \tag{17}$$

Because the pulse pair changes populations of the A levels *only*, it does not change the ratios N_A/N_E or N_{E^a}/N_{E^b}. Neither can it create dipolar energy which is proportional to the population difference $N_{A-3/2} + N_{A3/2} - N_{A-1/2} - N_{A1/2}$ but if there is some dipolar energy the pulse pair will decrease it by the factor $(1 - 2a - 2b)$.

If before the application of θ_x–t_1–θ_{-x} the system was at internal equilibrium described by the common spin temperature T, the excess populations will become

$$\begin{aligned}
n'_{A\pm3/2} &= \pm(\tfrac{3}{2} - a - 2b)\hbar\omega_0/8kT \\
n'_{A\pm1/2} &= \pm(\tfrac{1}{2} + a - 2b)\hbar\omega_0/8kT \\
n'_{E^a\pm1/2} &= n'_{E^b\pm1/2} = \pm\tfrac{1}{2}\hbar\omega_0/8kT
\end{aligned} \tag{18}$$

(with the same remarks concerning ω_t as mentioned in connection with the equation (13)). In this case the total nuclear magnetisation $\gamma\hbar\Sigma_{Xm}mN_{Xm}$ decreases by the factor $(1 - \frac{1}{3}a - \frac{4}{3}b)$ in accordance with the vector model.

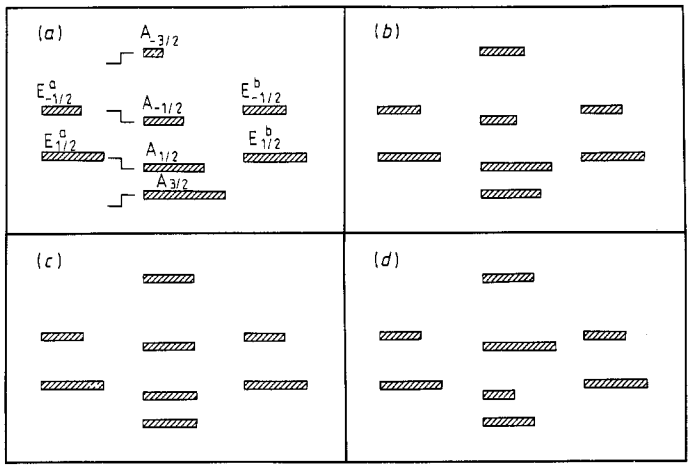

Figure 1. Energy-level populations of the three-spin system after the pulse pair θ_x–t_1–θ_{-x} with $t_1 = \pi\hbar/2d$ for four different values of θ (*a*) $\theta = 0°$; (*b*) $\theta = 45°$; (*c*) $\theta = 63.4°$; (*d*) $\theta = 90°$. The steps in the diagram for the thermal equilibrium or $\theta = 0°$ show the dipolar shifts $\pm d$ of the A levels.

The populations change most effectively if the interval t_1 between the pulses is made equal to $\pi\hbar/2d$. The populations of the non-equilibrium state (18) depend on the angle θ of the pulses. When $\theta = 90°$ these pulses make $N_{A1/2}$ maximally smaller than $N_{A-1/2}$ corresponding to a negative spin temperature of the inner A levels, and 45° pulses have the same effect on the populations of the outer A-level pairs. If $\theta = 63.4°$, all the A levels have a common spin temperature higher than the initial temperature T, which the E levels still have. For $\theta = 35.3°$ or 90° the temperature of the inner A levels differs most from T and for $\theta = 54.7°$ it is equal to T. Some cases are shown in figure 1.

The populations can be read by a third RF pulse. The form of the whole sequence is then θ_x–t_1–θ_{-x}–t_2–θ'. The time t_2 before the θ' pulse must be sufficiently long for the transverse magnetisation, produced by the preparing pulses, to decay practically to zero. The phase of the third pulse is immaterial because the off-diagonal components of the

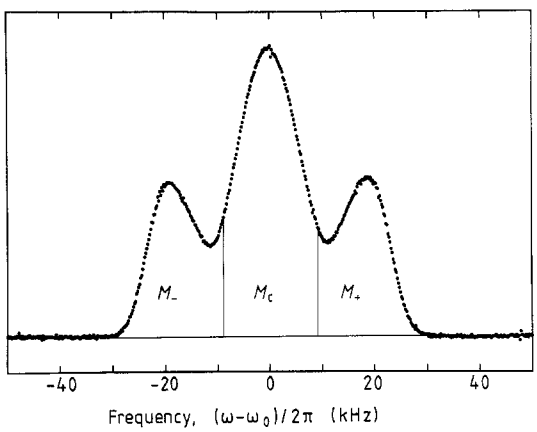

Figure 2. Proton equilibrium spectrum of a $CH_3COONa \cdot 3D_2O$ single crystal at 30 K. The external field of 0.76 T was parallel to the crystalline *c* axis. The marked areas are explained in § 3.2.

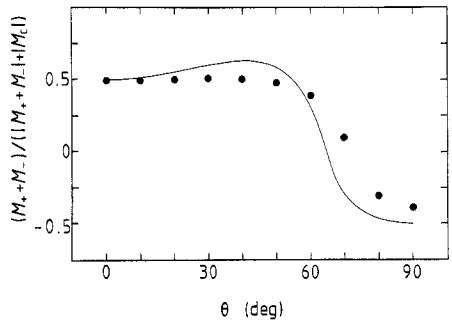

Figure 3. Experimental values for the ratio $(M_+ + M_-)/(|M_+ + M_-| + |M_c|)$ measured from sodium acetate spectra after the pulse sequence θ_x–26 μs–θ_{-x}–100 μs–90° at 30 K. The curve is calculated from equation (19) with $4d/h = 38$ kHz, $t_1 = 26$ μs, $\theta' = 90°$ and varying pulse angle θ.

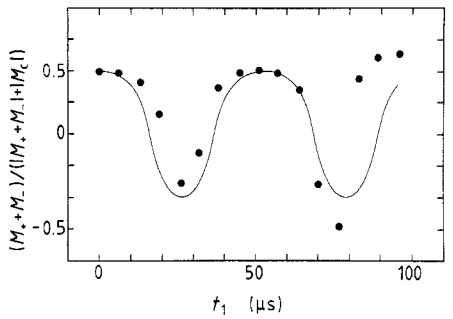

Figure 4. As figure 3, but for the sequence $90°_x$–t_1–$90°_{-x}$–100 μs–90°.

density operator have died out during t_2 as well. By replacing (11) by (18) we get from (9)

$$M_+ = M_- = [(3 - \tfrac{3}{2}a - \tfrac{9}{2}b)\sin\theta' + 3(b - a)\sin 3\theta'](\hbar\omega_0/16kT)$$
$$M_c = [(6 - a - 7b)\sin\theta' + 6(a - b)\sin 3\theta'](\hbar\omega_0/16kT). \tag{19}$$

In reality the populations start to readjust towards equilibrium immediately after the first two RF pulses. This development is caused partly by spin diffusion, partly by lattice-dependent relaxation. (We postpone the analysis of these processes to a later paper where we present results of our experiments on several samples in a wide temperature range.) From the FID after the θ' pulse one is able to calculate the populations at the moment t_2 by using the formulae (9) to (12). The pulse-angle dependence of the decay shape makes this determination possible because the shapes obtained with $\theta' = 90°$ and $\theta' \ll 90°$ give together more information than either alone. By varying the interval t_2, the time development of the system is then observed.

3. Experimental procedure

3.1. Sample and apparatus

An ideal sample for our purpose should contain identically oriented CH_3, CF_3 and NH_3 groups relatively isolated from each other. In real crystals which fulfill the first condition

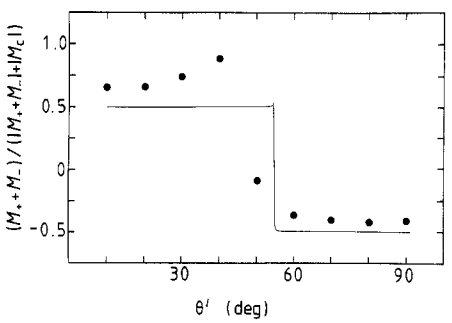

Figure 5. As figure 3, but for the sequence $90°_x$–26 μs–$90°_{-x}$–100 μs–θ'.

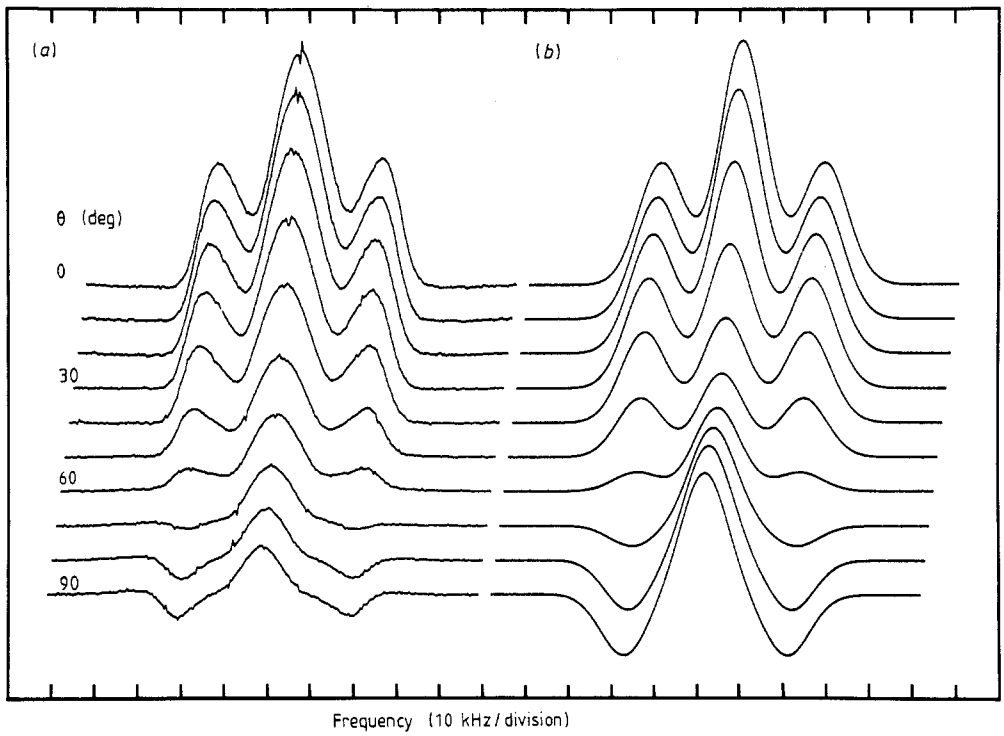

Figure 6. (*a*) Proton spectra of a $CH_3COONa \cdot 3D_2O$ single crystal at 30 K after the pulse sequence θ_x–26 μs–θ_{-x}–100 μs–90° for different angles θ from 0° to 90° in steps of 10°. (*b*) Theoretical spectra for the same sequence were calculated from equation (19) with $4d/h$ = 38 kHz and broadened by the Gaussian function with a FWHM of 12.5 kHz.

the groups are often arranged in coaxial pairs. The central line of the spectrum is then split by the dipole–dipole interaction between the nuclei of the two closely situated groups [16]. The splitting of the central line can be removed by orienting the crystal properly but for coaxial groups also the satellites collapse on the centre line at this same orientation.

The crystal structure of sodium acetate trihydrate is known from x-ray measurements [17]. The proton coordinates correspond to two differently oriented methyl groups with an angle of 126° between their axes. An NMR study on $CH_3COONa \cdot 3D_2O$ suggests that the axes are almost anti-parallel [18]. Moreover, the axis joining the two nearest neighbouring groups makes an angle of 18° with the axis of an individual methyl group. Therefore it is possible to eliminate the splitting of the central line without totally removing the satellite separation. Although the CH_3 reorientations become slow relative to the proton line width below 20 K, the A and E levels will not be mixed by the dipolar interaction even at the lowest temperatures because of the large tunneling splitting. In sodium acetate $\omega_t/2\pi$ is 1400 MHz at 4.2 K and still about 1100 MHz at 30 K according to inelastic neutron scattering [19].

Our single crystal of $CH_3COONa \cdot 3D_2O$ was grown from a supersaturated solution of CH_3COONa in the mixture of CH_3CH_2OD and D_2O. The orientation of the crystal was determined by reflecting laser light from the growth faces. The sample was partly ground to fit into the coil of 5 mm diameter. Our spectra confirmed the result of earlier NMR experiments that the maximum satellite separation with a reduced splitting of the

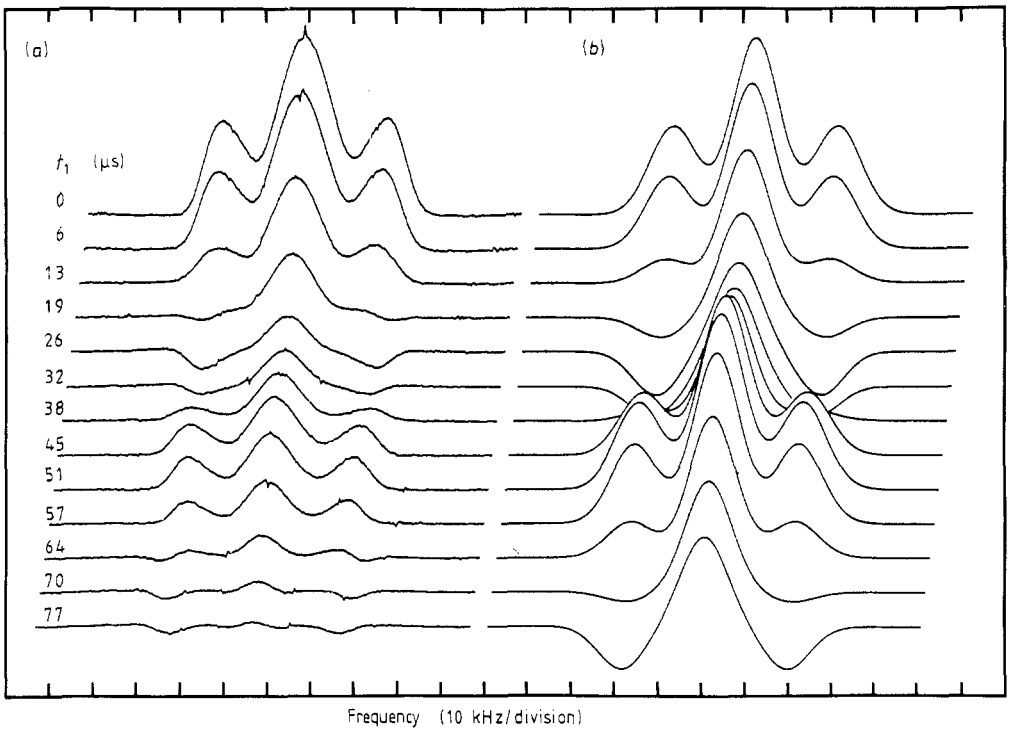

Figure 7. As figure 6 but for the sequence $90°_x$–t_1–$90°_{-x}$–100 μs–90° with different intervals t_1.

central line should appear when $\boldsymbol{B}_0$ is roughly parallel to the crystalline c axis [18]. This orientation, with 38 kHz separation between the satellites and 12.5 kHz FWHM of the central line, was used in all the experiments described here. The temperature 30 K near the T_1 minimum was chosen for being able to repeat the pulse sequence every 2 seconds. The effect of the pulses, however, was basically the same up to room temperature. The equilibrium spectrum is plotted in figure 2.

The experiments were carried out at the proton resonance frequency of 32.5 MHz by using a Thor superconducting magnet and a Bruker SXP 4-100 spectrometer. The pulse programmer and the accessories for the quadrature detection and the digital recording of the signals were constructed in our laboratory. The fast Fourier transform was performed with an ABC80 microcomputer. The probe and the cryostat for cooling by a liquid helium bath were also home-made.

3.2. Results and discussion

Figures 3 to 5 compare the equation (19) directly with measurements. The experimental values for M_+, M_- and M_c are the corresponding satellite and central line areas of the sodium acetate spectra at 30 K. The borderlines between the areas are shown in figure 2. They were chosen to make the ratio $(M_+ + M_-)/M_c$ equal to unity at thermal equilibrium. The original spectra are plotted in figures 6 to 8 together with their theoretical counterparts.

The curves in figures 3 to 5 are calculated from equations (17) and (19) by using the satellite separation $4d/h = 38$ kHz and also the experimental values for the parameters t_1, θ and θ'. The theoretical spectra in figures 6 to 8 are calculated from the same

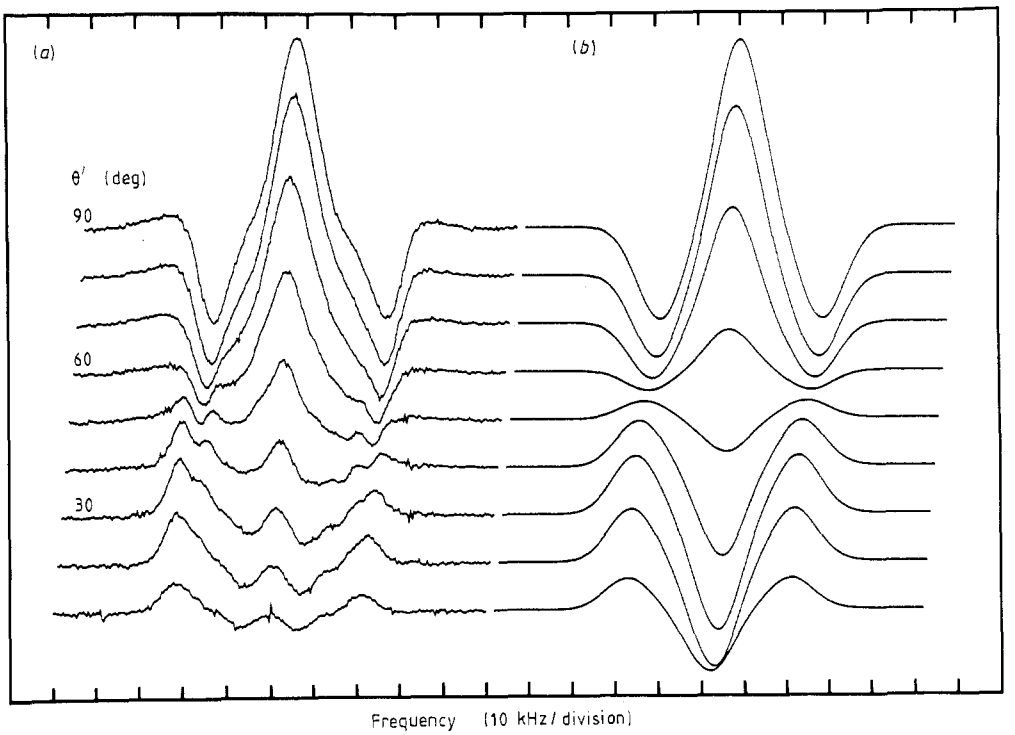

Figure 8. As figure 6 but for the sequence $90°_x$–26 μs–$90°_{-x}$–100 μs–θ' with different angles θ' from 10° to 90° in steps of 10°. Here the experimental spectra are magnified by the factor 2.5.

equations but are, in addition, broadened by the Gaussian function with a FWHM of 12.5 kHz width at the half intensity. In figures 6 and 7 the areas of the theoretical and the experimental spectra are made equal at thermal equilibrium. No other adjustable parameters are used. In figure 8, however, the experimental spectra are magnified by the factor 2.5 to show their structure more clearly.

The two series of experiments presented in figures 3 and 4 (and also in figures 6 and 7) demonstrate the effect of the pulse pair θ_x–t_1–θ_{-x} on the methyl-proton system. The points in figure 5 (or the spectra in figure 8) show the effect of the angle θ' of the measuring pulse. (The slight deviation of the curve from rectangular behaviour in figure 5 arises from a small difference between $t_1 = 26\ \mu s$ and $\pi\hbar/2d = 26.3\ \mu s$. Note the tendency of the experimental values to follow this curve.)

Generally, the theoretical and the experimental ratios $(M_+ + M_-)/(|M_+ + M_-| + |M_c|)$ agree rather well with each other. For thermal equilibrium the ratio is 0.5. The deviation of the theoretical curves and the experimental points from this value shows the effect of the A-level populations which do not obey a common spin temperature. The amplitudes of the experimental spectra or the absolute values of $M_\pm$ and M_c, however, are in many cases much less than expected by our model. This is mainly due to the exclusion of attenuation from our calculations during the interval t_1. The omission of the attenuation during the pulses is less serious because of their short duration of only 0.2–1.8 μs. Indirectly the pulse length has some effect because the degree to which the magnetisation is affected by attenuation depends on the angle θ of the pulses.

Another source for the difference between the theory and the experiment in the pulse sequence θ_x–t_1–θ_{-x}–t_2–θ' is the spin diffusion during the time t_2. To minimise this effect θ' should be applied as quickly as possible. The shortest safe value for t_2 depends on the angles of the pulses. For all our experiments the transverse magnetisation was observed to have decayed sufficiently in 100 μs.

Acknowledgments

We thank Mr M Komu, MSc, for building the hardware and most of the software for the Fourier analysis and Dr E E Ylinen for advice in experiments.

References

[1] Lowe I J and Norberg R E 1957 *Phys. Rev.* **107** 46
[2] Schäublin S, Höhener A and Ernst R R 1974 *J. Magn. Reson.* **13** 196
[3] Sørensen O W, Eich G W, Levitt M H, Bodenhausen G and Ernst R R 1983 *Prog. NMR Spectrosc.* **16** 163
[4] Vuorimäki A H, Punkkinen M and Ylinen E E 1987 *J. Phys. C: Solid State Phys.* **20** L749
[5] Freed J H 1965 *J. Chem. Phys.* **43** 1710
[6] Allen P S 1968 *J. Chem. Phys.* **48** 3031
[7] Lin C C and Swalen J D 1959 *Rev. Mod. Phys.* **31** 841
[8] Andrew E R and Bersohn R 1950 *J. Chem. Phys.* **18** 159
[9] Apaydin F and Clough S 1968 *J. Phys. C: Solid State Phys.* **1** 932
[10] Bloom M, Hahn E L and Herzog B 1955 *Phys. Rev.* **97** 1699
[11] Punkkinen M 1967 *Ann. Acad. Sci. Fenn.* A VI **239**
[12] Slichter C P 1980 *Principles of Magnetic Resonance* 2nd ed. (Berlin: Springer)
[13] Vuorimäki A H 1987 *Lic. Thesis* (in Finnish), University of Turku
[14] Goldman M and Shen L 1966 *Phys. Rev.* **144** 321
[15] Punkkinen M, Ylinen E E and Ingman L P 1982 *Phys. Rev.* B **26** 3943
[16] Allen P S 1978 *Faraday Symposia Chem. Soc.* **13** 133
[17] Wei K-T and Ward D L 1977 *Acta Crystallogr.* B **33** 522
[18] Punkkinen M, Meier B H and Ernst R R unpublished
[19] Clough S, Heidemann A and Paley M 1981 *J. Phys. C: Solid State Phys.* **14** 1001